3D ultrasound imaging with active instrumented needle tip tracking: An ex vivo study

Javad Rostami[1], Christian Baker[1], Weidong Liang[1], Simeon West[2], Tom Vercauteren[1], Sunish Mathews[3], Adrien Desjardins[3], Edward Zhang[3], Paul Beard[3], Sebastien Ourselin[2], Laura Peralta[1], Wenfeng Xia[1]

[1]School of Biomedical Engineering and Imaging Science, King's College London; [2]University College Hospital London; [3]University College London

***Abstract*—Ultrasound (US) imaging is widely used for guiding percutaneous needle procedures, but accurate visualisation of the needle tip and patient anatomy in 3D and in real-time is challenging. We introduce a system that integrates 3D US imaging with a needle tip tracking modality for guiding minimally invasive procedures such as nerve blocks and tumour biopsies. Using a 256-element sparse spiral array for real-time 3D imaging, the system also provides precise 3D tracking information of the needle tip with an integrated fibre-optic US sensor (FOS) that communicates with the US imaging probe. FOS data were beamformed to generate an image of the needle tip, precisely pinpointing its location on the B-mode images. The tracking accuracy of the systems was tested in a water tank using a 3D translation stage. The accuracy in the vertical direction (Z, depth) was 0.32 mm ± 0.16 mm (RMSE ± SD). In the lateral and elevational directions, the accuracies were 1.21 mm ± 0.55 mm and 0.63 mm ± 0.15 mm, respectively. The clinical translational potential of the system was further demonstrated with needle insertions into ex vivo chicken tissue. Future development aims to enhance image quality and tracking speed, offering significant advancements in the efficiency and safety of needle-based interventions.**

Keywords—needle tracking, sparse array, 3D imaging, minimally-invasive surgery, ultrasound imaging, ultrasound needle tracking, sparse array

I. Introduction

In procedures such as tumour biopsy, nerve blocks for regional anaesthesia, and fetal therapy, ultrasound (US) plays a critical role in guiding needle-based interventions [1]. Its real-time imaging capabilities allow clinicians to visualise the target area and monitor needle placement, enhancing precision and reducing the risk of complications. However, it faces challenges in accurately visualising the needle tip. Mispositioning needle tip risks severe complications such as pneumothorax, stroke and nerve damage [2].

US visualization of needles depends on how the needle scatters and reflects US waves. It is particularly challenging when needles are inserted at steep angles, as this can lead to a loss of visibility due to the direction of reflected US waves [3]. Furthermore, the process is complicated by artefacts such as reverberations and side lobes [4]. These artefacts, combined with visibility being compromised at greater depths due to tissue-related acoustic attenuation [5], pose additional challenges to accurate needle tracking. While various methods have been suggested to improve the visibility of the needle on the B-mode imaging plane such as modifying the needle surface to increase specular reflection [3], using image processing techniques [6], or beam steering [7], accurately pinpointing the exact location of the needle tip remains a significant challenge. One approach to addressing this issue is to use a sensor, such as electromagnetic [8] or piezoelectric, at the needle tip [9]. The data from the sensor is processed and integrated into the B-Mode image to show the needle tip position. A major drawback of electromagnetic sensors is their vulnerability to interference from electromagnetic fields. This interference can come from everyday objects like metal tables and instruments, which significantly reduces their accuracy. Furthermore, these sensors often require large external components [2]. Current piezoelectric US sensors may be less effective. This is partly due to the difficulty of integrating them into small-diameter needles [2]. Alternatively, a fibre-optic sensor (FOS) can offer reduced size and flexibility for easier integration into the needle and has the potential for higher sensitivity and resolution[8], [10], [11]. In those previous works, the FOS had a Fabry-Pérot cavity at its distal end. This cavity consisted of a polymer spacer between two reflective layers with a 150 μm outer diameter. The optical reflectivity of the cavity changed with incident acoustic pressure [12]. Meanwhile, artificial intelligence (AI) methods such as deep learning could be used to enhance US needle tracking [13]. One of the greatest challenges is the 2D nature of B-Mode images generated by 1D US probes. If the needle moves out of this 2D plane, its tip might become invisible, which could lead to mistakenly identifying the point where the needle shaft intersects the imaging plane as the tip [8].

Real-time volumetric US imaging can address this issue, provided the needle remains within the imaging volume [14]. In addition, 3D ultrasound provides a comprehensive view of the anatomy, allowing for better spatial understanding of structures and pathology, which is crucial for precise needle placement. However, 2D matrix arrays usually require complex systems. Sparse arrays effectively reduce both the number of active elements and the amount of received data to be stored and processed, which allows systems less demanding of hardware electronics[15].

In this work, we propose integrating the use of an FOS at the needle tip and combine it with an external 2D sparse spiral array to improve needle tracking in US-guided interventions. Together, these advancements represent a significant leap forwards in US-guided needle procedures. They promise enhanced accuracy, reduced risk of needle misplacement, and increased success rates for medical interventions by ensuring precise needle placement within a 3D anatomical context.

II. Materials and Methods

A. Ultrasound Imaging

A 256-element spiral sparse array connected to an ultrasound advanced open platform (ULA-OP 256) was used for real-time US imaging [16]. The design of the sparse array

This work was supported by core funding from the Wellcome/EPSRC Centre for Medical Engineering [WT203148/Z/16/Z] and The Royal Society [URF/R1/211049].

was adopted using a 1024-element matrix array arranged in a 32 × 35 grid (sourced from Vermon S.A., Tours, France) [14], [17] (Fig. 1). The layout leaves certain rows (9, 18, and 27 in the y-direction) disconnected to satisfy specific routing requirements The array had a central frequency of 3.7 MHz and 60% bandwidth with an element pitch of 300 × 300 µm. 256 elements were selected based on an ungridded, 10.4-mm-wide spiral with 256 seeds, whose density tapering was modulated according to a 50% Tukey window [18](see Fig. 1).

At a pulse repetition frequency (PRF) of 1000 Hz, imaging was performed by transmitting steered plane waves (PWs), obtained with four-cycle Gaussian pulses at the 3-MHz centre frequency. A total of nine PWs were transmitted at various steering angles by incrementing in 2.5° steps, both in the lateral (X) and elevational (Y) directions, up to a maximum steering angle of ±5°. The specific steering angles used for transmission are listed in Table I.

Table I. Steering angles used for US transmission

Lateral (X-axis) Angle [°]	**Elevation (Y-axis) Angle [°]**
-5.0	0
-2.5	0
0	0
2.5	0
5.0	0
0	-5.0
0	-2.5
0	2.5
0	5.0

positioning the tip at the clinical target. The FOS featured a Fabry-Pérot cavity at its distal end, consisting of a polymer spacer between two reflective layers with an outer diameter of 150 µm. The optical reflectivity of this cavity changed in response to incident acoustic pressure [12]. The Fabry-Pérot cavity was probed using a wavelength-tunable laser (1500nm to 1600nm, TSL-550, Santec, Komaki, Japan). The reflected light was sent to a photo-detector, which generated a voltage that corresponded to the cavity's changing reflectivity and hence the acoustic pressure. A data acquisition card (M2p.5961-x4, Spectrum Instrumentation GmbH, Großhansdorf, Germany) acquired this voltage by the photo-detector. The schematic of the system is demonstrated in Fig.1.

For tracking, the 256 elements in the sparse spiral array sequentially transmitted a four-cycle Gaussian pulse at 3 MHz centre frequency. The data acquisition card was programmed to start acquiring 2048 samples right after each triggering event in the ULA-OP 256 scanner with a sampling rate of 25 MHz. Data acquisition continued until the user terminated the Spectrum digitizer's programme, which meant real-time data acquisition was achieved. Considering 9 triggering events used for US imaging and 256 events used for tracking, 265 triggering events were used for one frame. Thus the system's frame rate was 3 frames per second.

As a result, each frame comprised two separate data sets: US images from the sparse spiral array and data from the FOS at the needle tip. In the tracking data set, for each frame, there were 256 tracking waveforms. These waveforms are bandpass-filtered beamformed by the DAS algorithm to estimate the location of the needle tip using maximum intensity projection and pinpoint the needle tip on the B-mode images. Samples of both data sets are demonstrated in Fig 2.

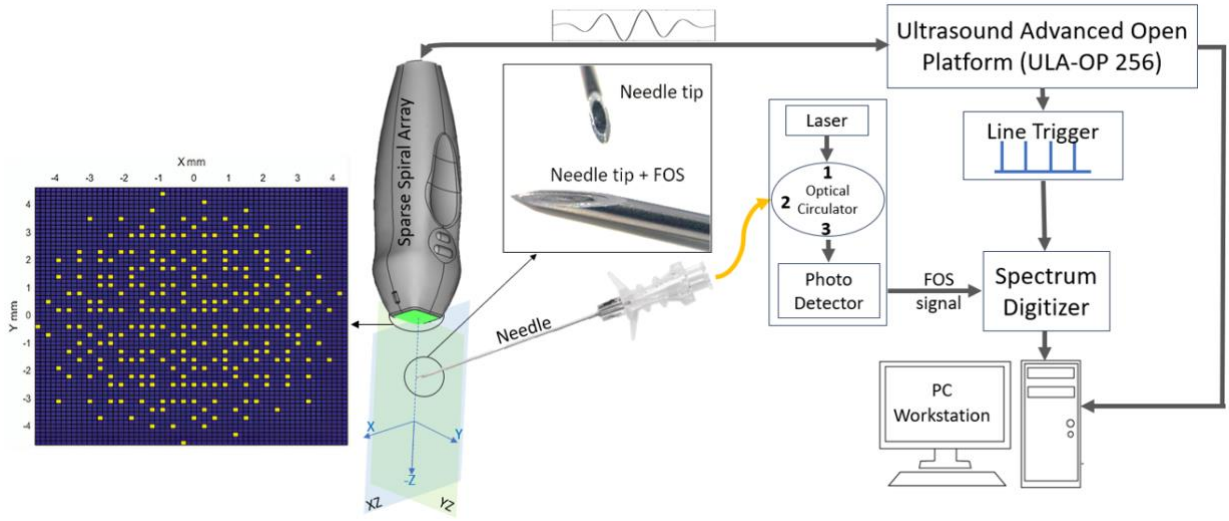

Fig 1. Schematic diagram of 3D US imaging and Tracking and the layout of the 2D sparse spiral array

The recorded data after being band-pass filtered were beamformed using the delay and sum (DAS) algorithm.

B. Needle Tip Tracking

A 20 gauge, 150mm long needle cannula was used, with an FOS integrated into the stylet (Fig.1). The stylet and FOS were designed to be removed from the cannula after

C. Accuracy Assessment

To assess accuracy, the probe was mounted vertically downwards and partially immersed in a water tank, while the needle was held horizontally beneath the probe and moved using a 3D automated translation stage. The temperature of

the water was monitored during the experiment and it was 22±0.5 °C. Data were recorded across 4 depths; 10 mm, 20 mm, 30 mm, and 40 mm. At each depth, 16 lateral/elevational points on a 2 mm grid were recorded and compared with the ground truth from the translation stage. For each point, 18 frames were recorded. For accuracy assessment, only the tracking data were considered. For each point, the data were beamformed and the index of the voxel with the greatest value was taken as the location of the needle tip. At each position, the tracking accuracy was defined as root mean squared error (RMSE) from all data points against values from the 3D translation stage within the interval of standard deviation (SD).

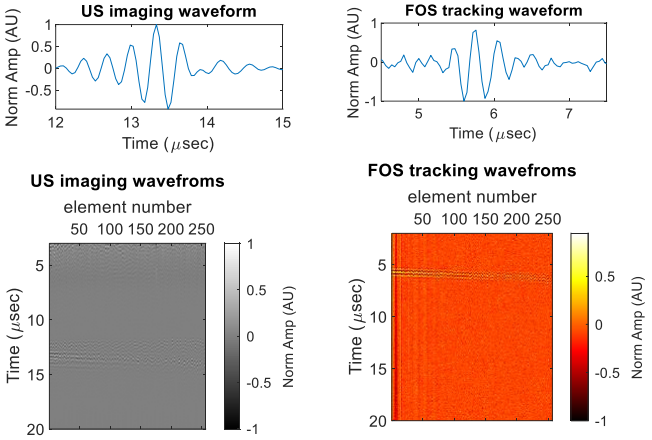

Fig 2. Samples of raw US imaging waveforms (left) and FOS tracking waveforms (right)

D. Ex vivo study

The performance of the system was validated ex vivo using chicken breast tissue. A clear silicon tube (ID: 0.5 mm; OD:1mm) was embedded into the chicken breast and filled with water to represent a tumour inside a tissue. This setup aimed to validate the system's ability to visualise complex structures within the tissue, as well as to track the needle tip accurately. The needle was inserted into the tissue at a depth of approximately 10 mm and an insertion angle of approximately 15°.

III. Results, Discussion and Conclusion

The accuracy assessment test results showed that the total accuracy in the vertical direction (Z, depth) was 0.32 mm ± 0.16 mm (RMSE ± SD). In the lateral and elevational directions, the accuracies were 1.21 mm ± 0.55 mm and 0.63 mm ± 0.15 mm, respectively.

The results of the ex vivo experiment are shown in Fig. 3, where Fig. 3(a) presents the *xy* and *yz* plane B-mode ultrasound images, and Fig. 3(b) displays the tracking data images.

The 3D structure of the tissue in Fig. 3(a) shows two bright regions with high reflectivity. These likely correspond to the water-filled tube, representing a tumour, and the needle. However, identifying the needle tip in the US image is challenging. In contrast, the tracking images in Fig. 3(b) clearly show a bright spot at the needle tip, representing the position of the FOS. The voxel with the highest value was identified and marked with a cross to indicate the needle tip. It was located at X = -0.67mm, Y= -1.87mm and Z=9.00mm This cross was then overlayed onto the US images in Fig. 3(a) at the same location.

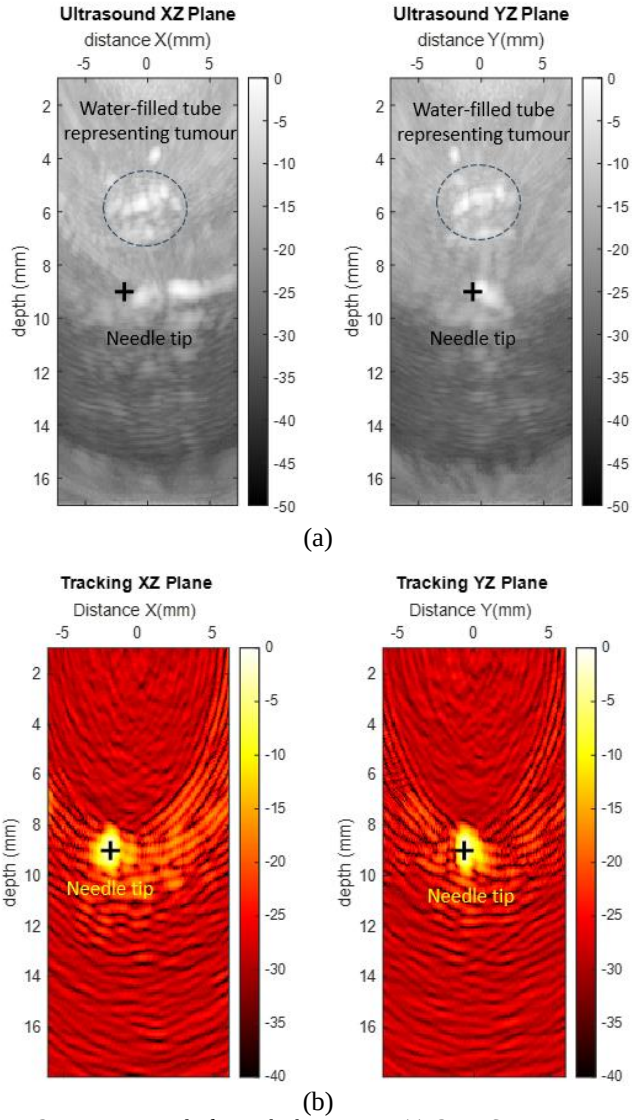

Fig. 3. Ex vivo result from chicken tissue: (a) 3D US images in two perpendicular planes that contain the needle and the water-filled tube inside the tissue. The cross on the image shows the needle tip. (b) Beamforming results of the tracking data showing the location of the needle tip.

In Fig. 3(a), the needle tip (marked by the cross) does not always align with a bright spot. This could be because the bright spot next to the cross represents another structure within the tissue. Additionally, unlike the needle shaft, the reflection from the tip may be weaker. These results highlight the value of FOS tracking data in identifying the needle tip in US images.

While sparse arrays may not match to produce images with the same quality as those generated by 2D dense arrays with the same aperture and element size, they can produce images with reasonable quality without the need for cumbersome cable connections to complex high-channel count scanners. Furthermore, reduced element number in the sparse spiral array helps with achieving a higher frame rate in data acquisition and saves computational costs in image reconstruction and tracking algorithms. They represent a

feasible option for 3-D imaging and 3D needle tracking at a moderate cost.

For tracking, unlike electromagnetic solutions, the FOS does not require a bulky field generator near the clinical site. It also remains unaffected by ferromagnetic materials in the surgical area. FOS easily fits inside the intraoperative needle. In contrast, piezoelectric systems require custom needles with integrated electrical connections and a small enough element to fit at the needle tip. Moreover, FOS features a broadband frequency response with high sensitivity up to at least 50 MHz that is compatible with ultrasound imaging probes with a wide range of frequency bandwidths. In contrast, many piezoelectric elements have a narrow response. Plus, while smaller piezoelectric elements broaden directivity but lower sensitivity, FOS has a small active area, that offers broad directivity. This reduces the impact of needle angle on tracking variance while maintaining sensitivity.

This innovation represents a promising tool for enhancing safety and efficacy in various minimally invasive procedures.

REFERENCES

[1] S. Park, D. G. Beom, E. H. Bae, S. W. Kim, D. J. Kim, and C. S. Kim, "Model-Based Needle Identification Using Image Analysis and Needle Library Matching for Ultrasound-Guided Kidney Biopsy: A Feasibility Study," *Ultrasound Med. Biol.*, vol. 49, no. 8, pp. 1699–1708, Aug. 2023, doi: 10.1016/j.ultrasmedbio.2023.03.009.

[2] W. Xia *et al.*, "In-plane ultrasonic needle tracking using a fiber-optic hydrophone," *Med. Phys.*, vol. 42, no. 10, pp. 5983–5991, Oct. 2015, doi: 10.1118/1.4931418.

[3] C. H. Hovgesen, J. E. Wilhjelm, P. Vilmann, and E. Kalaitzakis, "Echogenic Surface Enhancements for Improving Needle Visualization in Ultrasound," *J. Ultrasound Med.*, vol. 41, no. 2, pp. 311–325, Feb. 2022, doi: 10.1002/jum.15713.

[4] G. Reusz, P. Sarkany, J. Gal, and A. Csomos, "Needle-related ultrasound artifacts and their importance in anaesthetic practice," *British Journal of Anaesthesia*, vol. 112, no. 5. Oxford University Press, pp. 794–802, 2014. doi: 10.1093/bja/aet585.

[5] K. J. Chin, A. Perlas, V. W. S. Chan, and R. Brull, "Needle Visualization in Ultrasound-Guided Regional Anesthesia: Challenges and Solutions," *Regional Anesthesia and Pain Medicine*, vol. 33, no. 6. pp. 532–544, Nov. 2008. doi: 10.1016/j.rapm.2008.06.002.

[6] P. Beigi, S. E. Salcudean, G. C. Ng, and R. Rohling, "Enhancement of needle visualization and localization in ultrasound," *Int. J. Comput. Assist. Radiol. Surg.*, vol. 16, no. 1, pp. 169–178, Jan. 2021, doi: 10.1007/s11548-020-02227-7.

[7] C. R. Hatt, G. Ng, and V. Parthasarathy, "Enhanced needle localization in ultrasound using beam steering and learning-based segmentation," *Comput. Med. Imaging Graph.*, vol. 41, pp. 46–54, Apr. 2015, doi: 10.1016/j.compmedimag.2014.06.016.

[8] C. Baker *et al.*, "Intraoperative Needle Tip Tracking with an Integrated Fibre-Optic Ultrasound Sensor," *Sensors*, vol. 22, no. 23, Dec. 2022, doi: 10.3390/s22239035.

[9] F. Winsberg, H. A. Mitty, R. S. Shapiro, and H. C. Yeh, "Use of an acoustic transponder for US visualization of biopsy needles," *Radiology*, vol. 180, no. 3, pp. 877–878, 1991, doi: 10.1148/radiology.180.3.1871312.

[10] W. Xia *et al.*, "Coded excitation ultrasonic needle tracking: An in vivo study," *Med. Phys.*, vol. 43, no. 7, pp. 4065–4073, Jul. 2016, doi: 10.1118/1.4953205.

[11] S. J. Mathews *et al.*, "Ultrasonic Needle Tracking with Dynamic Electronic Focusing," *Ultrasound Med. Biol.*, vol. 48, no. 3, pp. 520–529, Mar. 2022, doi: 10.1016/j.ultrasmedbio.2021.11.008.

[12] J. A. Guggenheim *et al.*, "Ultrasensitive plano-concave optical microresonators for ultrasound sensing," *Nat. Photonics*, vol. 11, no. 11, pp. 714–719, Nov. 2017, doi: 10.1038/s41566-017-0027-x.

[13] E. Maneas *et al.*, "Enhancement of instrumented ultrasonic tracking images using deep learning," *Int. J. Comput. Assist. Radiol. Surg.*, vol. 18, no. 2, pp. 395–399, 2023, doi: 10.1007/s11548-022-02728-7.

[14] L. Peralta, D. Mazierli, A. Gomez, J. V. Hajnal, P. Tortoli, and A. Ramalli, "3-D Coherent Multitransducer Ultrasound Imaging With Sparse Spiral Arrays," *IEEE Trans. Ultrason. Ferroelectr. Freq. Control*, vol. 70, no. 3, pp. 197–206, Mar. 2023, doi: 10.1109/TUFFC.2023.3241774.

[15] A. Ramalli, E. Boni, E. Roux, H. Liebgott, and P. Tortoli, "Design, Implementation, and Medical Applications of 2-D Ultrasound Sparse Arrays," *IEEE Trans. Ultrason. Ferroelectr. Freq. Control*, vol. 69, no. 10, pp. 2739–2755, 2022, doi: 10.1109/TUFFC.2022.3162419.

[16] E. Boni *et al.*, "ULA-OP 256: A 256-Channel Open Scanner for Development and Real-Time Implementation of New Ultrasound Methods," *IEEE Trans. Ultrason. Ferroelectr. Freq. Control*, vol. 63, no. 10, pp. 1488–1495, Oct. 2016, doi: 10.1109/TUFFC.2016.2566920.

[17] A. Ramalli *et al.*, "High-frame-rate tri-plane echocardiography with spiral arrays: From simulation to real-time implementation," *IEEE Trans. Ultrason. Ferroelectr. Freq. Control*, vol. 67, no. 1, pp. 57–69, Jan. 2020, doi: 10.1109/TUFFC.2019.2940289.

[18] A. Ramalli, E. Boni, A. S. Savoia, and P. Tortoli, "Density-tapered spiral arrays for ultrasound 3-D imaging," *IEEE Trans. Ultrason. Ferroelectr. Freq. Control*, vol. 62, no. 8, pp. 1580–1588, Aug. 2015, doi: 10.1109/TUFFC.2015.007035.